PERGAMON

International Journal of Heat and Mass Transfer 41 (1998) 3989–4007

International Journal of HEAT and MASS TRANSFER

Experimental analysis of a confined transitional plume with respect to subgrid-scale modelling

Rob J. M. Bastiaans*, C. C. M. Rindt, A. A. van Steenhoven

J.M. Burgers Centre for Fluid Dynamics, Eindhoven University of Technology, Department of Mechanical Engineering, P.O. Box 513, 5600 MB Eindhoven, The Netherlands

Received 12 August 1997; in final form 3 February 1998

Abstract

Free convection flow of water induced by a small prismatic heat source in a confined space is studied in the present paper. The forcing of the flow is in the range of Rayleigh numbers where a spatial transition from laminar to turbulent flow can be observed.

Velocity measurements were performed by means of Particle Tracking Velocimetry (PTV). From the velocity data a resolved and a subgrid field is obtained by means of spatial filtering. These data are analysed with respect to modelling consequences in Large-Eddy Simulation (LES), constituting an a priori test.

A statistically steady flow has been obtained with a converged temporal mean and standard deviation as function of space. A low correlation of time mean model stresses with exact stresses is found. In the transitional region the inter-scale kinetic energy transfer, taken over a wavenumber corresponding to the laminar plume width, is found to possess a relative large standard deviation. In this region backscatter and forward scatter of kinetic energy, with respect to the mentioned wavenumber, are of equal importance. Application of a dynamic model to the filtered data yields a qualitative good representation of the exact inter-scale kinetic energy transfer.

Nomenclature

A area
c_p constant pressure heat capacity
C model parameter
C_{ij} cross stresses
d_p particle diameter
D domain depth
f any quantity
$\bar{f}, \hat{f}$ filtered quantity
$\langle f \rangle$ time averaged value
f' subgrid quantity
f'' temporal standard deviation
g convolution kernel
g_i gravitational acceleration
h_i subgrid heat flux
H domain height
K_h eddy diffusivity
K_m eddy viscosity
L_{ij} Leonard stresses
$\mathscr{L}_{ij}$ test window stress
M_{ij} dynamic scaling tensor
p pressure
Pr Prandtl number
Pr_t turbulent Prandtl number
q' heat flux per unit length
q'' heat flux per unit area
q''' heat flux per unit volume
r_f radius of test area
R_{ij} Reynolds stresses
Ra Rayleigh number
S_{ij} rate of deformation tensor
t time
T temperature
u_i velocity component
V volume
W domain width
x_i spatial coordinate.

Greek symbols
α heat transfer coefficient

* Corresponding author. E-mail: r.j.m.bastiaans@wtb.tue.nl

0017–9310/98 $19.00
PII: S0017–9310(98)00075–1

β expansion coefficient
δ_{ij} Kronecker delta
Δ difference, grid-size
ε inter-scale kinetic energy transfer
κ thermal diffusivity
λ thermal conductivity
μ mean value
ν kinematic viscosity
ρ fluid density
ρ_p density of particles
σ standard deviation
τ_{ij} subgrid stress
Ω domain.

1. Introduction

This paper deals with the analysis of a transitional plane plume flow in a confined geometry, originating from a small prismatic source. This results in a complex buoyancy induced flow. Two- and three-dimensional flow features are present as well as a large separation of relevant length scales. Because of the confinement any similarity approach exhibits only a very limited relevance. From an engineering point of view the behaviour of this flow is very interesting. It is responsible for the thermal conditions in boilers and electronic equipment and determines in these situations the performance of the storage of heat and durability, respectively.

Fully developed conditions of plane plumes in unbounded space are well documented in the literature. The laminar variant is described by [12] on the basis of similarity conditions. The behaviour of turbulent plane plumes was reported by the experimental study of [28]. An integral (similarity) model for this situation is provided by the entrainment hypothesis of [29]. Furthermore the stability of plane plumes in unbounded space was investigated numerically by [25], in which also supporting results of additional experiments are given. More extended experiments were performed by [3], who examined the transition to turbulence in more detail. Most of the results mentioned are collected in [11].

Yet, not much information is available about the behaviour of plane plumes in a confined geometry. This might be due to the presence of sensitively interacting complex features and the large scale separation which makes it hard to obtain converged statistics. Because of the sensitivity of boundary and initial conditions useful data are provided only recently by Direct Numerical Simulations (DNS). Thus, the 2-D case was studied by [7] and [20] and the 3-D case by [2].

On the one hand the calculation of these 3-D flows by means of DNS requires a large computer capacity. On the other hand to perform parametric studies on such flows for engineering purposes, the use of computational solution techniques cannot be avoided. Because of the sensitivity of the transitional flow to low frequency and low amplitude large scale motions, as indicated by [25], it is important to perform unsteady calculations. This feature is the reason why the use of a LES technique could be the most appropriate method of calculating the flow.

The LES technique is meant to simulate flows at relative large forcing rates. This is done by reducing the spatial sample resolution that would be required for performing a DNS. Application of such a coarse spatial sampling grid to the flow results in an unresolved flow field. However, interactions in which unresolved flow scales participate may influence the flow field at the grid-scale. Therefore a SubGrid Model (SGM) has to be introduced, accounting for these influences. An LES requires a proper SGM that parameterizes the subgrid stresses and subgrid heat fluxes sufficiently well. Simulations with such a model are able to produce physically significant results at a relative low computational effort.

The present study focusses on plume flows that are buoyancy induced and originate from discrete sources. In such flows a spatial transition from laminar to turbulent flow is accompanied by relatively low (buoyant) forcing rates. Therefore the turbulent dissipation is small. On the other hand the scale separation is relatively large. This is why the application of LES is an attractive way of dealing with this flow. Furthermore, the resulting flow is highly non-homogeneous, a feature that additionally has its reflections on the degree of local isotropy and thus on modelling difficulties.

The objective of this study is to gain insight into the transitional behaviour of buoyant plumes. This with respect to modelling consequences in case of employment of LES. Therefore, an experiment is performed.

Most analyses on subgrid scale modelling and practical realizations of LES as documented in the literature, are concerned with forced flows. Most frequently these flows exhibit a relatively large turbulent dissipation rate. Then the classical Smagorinsky model, as described in [16], performs fairly well, except in the neighbourhood of solid walls. In general it can be stated that in the application of LES problems appear in the presence of a transition from laminar to turbulent flow. This is the case in the present transitional flow configuration as well as in turbulence near solid walls. In the case of fully turbulent channel flow, both [6] and [21], are examples of the successful application of the Smagorinsky model, on a relative coarse and fine grid, respectively.

Contrary to these successes, capturing of a spatial transition is not a trivial affair. Adapting model constants to the local behaviour of the flow in a dynamic way could be a solution. This is pioneered in [13] by establishing the 'dynamic model'. However, this is not always a satisfactory procedure as will be shown. One of the recent successful results on the basis of an alternative method is given in [9] for the spatial transition of a purely forced

boundary layer flow on a flat plate. In this study a spatial high-pass filter is applied to the grid-scale velocity field before evaluating the 'structure function' eddy viscosity model. This results in a sensitive dependence of the model on the smallest resolved scales of motion.

In thermal convective flows an extra complication is provided by the interaction of the velocity and temperature field and the accompanying coupling of the closure assumptions for both processes. A standard way of treating the coupling is the application of a turbulent Prandtl number, though its value is not well established. Dynamic versions of the coupling are given in [17] (revised in [2]) and [32], but these cannot be applied directly in the case of spatially transitional plumes as will be shown.

The SGM, that potentially may be applied to the flow phenomena under consideration, are validated by means of experimental data. The experimental technique used in the present study to obtain field information of the velocity is PTV.

In this paper first the fundamentals of LES will be addressed together with the methods of testing an SGM. This is followed by a description of the experiment. The experimental setup will be discussed, after which the experimental conditions are documented. An extensive description of the PTV measurement technique is provided, as it is applied in the present study. After this the data analysis for the present purpose is addressed. The subsequent section is a presentation of the obtained results. The paper ends with a summary of the major conclusions.

2. Large-eddy simulation

The starting point is the Boussinesq approximation for the equations of the conservation of mass, momentum, and internal energy. The basis of the theory of LES consists of the application of a spatial convolution filter to the governing equations. This procedure splits a generic turbulent variable f into a large scale component $\bar{f}$, and a subgrid component f'. The decomposition and the convolution of f with a filter function g over the flow domain Ω are given by

$$f(x_i,t)=\bar{f}(x_i,t)+f'(x_i,t) \tag{1}$$

where

$$\bar{f}(x_i,t)=\int_{\Omega} g(x_i-x_i')f(x_i',t)\,\mathrm{d}x_i'. \tag{2}$$

The filter function g has to satisfy the normalization condition, $\int_{\Omega} g(x_i-x_i')\,\mathrm{d}x_i'=1$.

Application of the filter to the governing equations yields a description of the large-scale motion according to

$$\frac{\partial \bar{u}_i}{\partial x_i}=0 \tag{3}$$

$$\frac{\partial \bar{u}_i}{\partial t}+\frac{\partial}{\partial x_j}(\bar{u}_i\bar{u}_j)=-\frac{\partial \bar{p}}{\partial x_i}+\nu\frac{\partial^2 \bar{u}_i}{\partial x_j^2}+g_i\beta\overline{\Delta T}-\frac{\partial \tau_{ij}}{\partial x_j} \tag{4}$$

$$\frac{\partial \bar{T}}{\partial t}+\frac{\partial}{\partial x_j}(\bar{u}_j\bar{T})=\kappa\frac{\partial^2 \bar{T}}{\partial x_j^2}+\frac{\overline{q'''}}{\rho c_p}-\frac{\partial h_j}{\partial x_j} \tag{5}$$

where $\kappa=\lambda/(\rho c_{\mathrm{p}})$ is the thermal diffusivity. All fluid properties are taken at the reference temperature at which the coefficient of thermal expansion is defined. The reference temperature level from which ΔT is the deviation may be defined at any value. The subgrid stresses and fluxes are then defined by

$$\tau_{ij}=\overline{u_iu_j}-\bar{u}_i\bar{u}_j \quad \text{and} \quad h_j=\overline{u_jT}-\bar{u}_j\bar{T} \tag{6}$$

respectively. These are commonly modelled on the basis of a gradient diffusion concept and coupled by a turbulent Prandtl number,

$$\tau_{ij}=-2K_{\mathrm{m}}\bar{S}_{ij}, \quad h_j=-K_{\mathrm{h}}\frac{\partial \bar{T}}{\partial x_j} \quad \text{and} \quad Pr_{\mathrm{t}}=\frac{K_{\mathrm{m}}}{K_{\mathrm{h}}}. \tag{7}$$

This introduces an eddy viscosity K_{m} and an eddy diffusivity K_{h}. For a given turbulent Prandtl number Pr_t only the eddy viscosity has to be parametrized in terms of resolved quantities. However, the value of Pr_{t}, typically $\frac{1}{3}<Pr_{\mathrm{t}}<\frac{1}{2}$ (see [10]), is not well established for any flow. The stresses τ_{ij} can be decomposed in a sum of Leonard stresses L_{ij}, cross stresses C_{ij}, and Reynolds stresses R_{ij} defined by

$$L_{ij}=\overline{\bar{u}_i\bar{u}_j}-\bar{u}_i\bar{u}_j, \quad C_{ij}=\overline{\bar{u}_iu_j'}+\overline{u_i'\bar{u}_j}, \quad \text{and} \quad R_{ij}=\overline{u_i'u_j'}. \tag{8}$$

In the present paper only the momentum closure is considered. Two models are taken into account, the classical Smagorinsky model ([16]) as given by

$$K_{\mathrm{m}}=C\Delta^2|\bar{S}| \tag{9}$$

and the standard dynamic model, according to [13], in the formulation of [17], in which the constant C of expression (9) is evaluated dynamically according to

$$C=\frac{1}{2}\frac{\mathscr{L}_{ij}M_{ij}}{M_{kl}M_{kl}}. \tag{10}$$

The test window stresses $\mathscr{L}_{ij}$ and M_{ij} are defined by

$$\mathscr{L}_{ij}=\widehat{\bar{u}_i\bar{u}_j}-\hat{\bar{u}}_i\hat{\bar{u}}_j \quad \text{and} \quad M_{ij}=\Delta^2|\widehat{\bar{S}}|\widehat{\bar{S}}_{ij}-\hat{\Delta}^2|\hat{\bar{S}}|\hat{\bar{S}}_{ij}, \tag{11}$$

respectively. The hat operator $\widehat{\ }$ denotes a low-pass filtering with a kernel of size $\hat{\Delta}=2\Delta$.

3. Subgrid stresses and their validation

Validation of subgrid models with the experimentally obtained data can be performed in two ways, generally

referred to as a priori testing on the one hand and a posteriori testing on the other hand; a denotation as introduced in [27].

A direct comparison of the experimental results with those obtained by an LES, using a particular subgrid-scale model, is generally referred to as a posteriori testing. The term a posteriori testing is also used if the reference data are generated by Direct Numerical Simulation (DNS). The process of a posteriori testing is the standard way to evaluate a model.

The other method, a priori testing, employs the reference data to pronounce directly upon the quality of a subgrid model. In this case the high resolution reference data are filtered spatially. Using the data at the two resolution levels, subgrid stresses are calculated. These stresses are then compared to the subgrid stresses determined with a model acting on the filtered data. Thus, the performance of several models can be evaluated, and suitable candidates can be discerned for actual large-eddy simulations. However, a good agreement between the real stresses and the stresses as obtained by using a model is not a guarantee for a successful LES. In an LES the SGS model affects the resulting resolved velocity and temperature field. The latter is taken as an input for evaluating the model. As a consequence a discrepancy between experimental data and LES data is likely to occur. The different sets of input data should converge with improvement of the model.

The a priori method, employed on the basis of DNS data, was pioneered in [4] and [19]. At present it has become a widely used investigation tool. However, using DNS data restricts the test to relatively low forcing rates, i.e. low Reynolds numbers or, as in the present case, low Rayleigh numbers. One of the first extensive studies based on experimental data at relatively high Reynolds numbers is documented in [18]. A drawback of the latter study, in comparison to the studies using DNS data, is the fact that only 2-D fields were used. Contrary to the flow conditions as investigated in the present study, it must be stressed that the majority of a priori testing so far has again been performed on forced convection, in which there are at least two homogeneous directions.

This paper describes the direct results of the experiment as well as an a priori analysis of the flow, focussing on the inter-scale kinetic energy transfer. With the filtered velocity field the rate of strain tensor $\bar{S}_{ij}$ can be calculated at the filtered level using a straightforward finite difference scheme. The rate of strain tensor, together with the subgrid scale stresses, define the inter-scale kinetic energy transfer. It can be written as function of the filter width,

$$\varepsilon(2\Delta) = -\tau_{ij}\bar{S}_{ij}. \tag{12}$$

If $\varepsilon(2\Delta)$ is positively valued, the kinetic energy is drained from the resolved scale to the subgrid scale. This should be the case if an inertial subrange is present.

4. The experiment

4.1. *The experimental setup*

A schematic drawing of the setup is given in Fig. 1. The dimensions of the flow domain are taken to be $W \times H \times D = 0.3 \times 0.2 \times 0.2$ m^3. In the domain an electrical heating element is mounted, which has the form of a strip of size $W \times H \times D = 0.002 \times 0.02 \times 0.2$ m^3. It is positioned in the symmetry plane, its lower side at a height of 0.01 m. At the operating heat flux (as given in the next section), the element's surface is sufficiently large

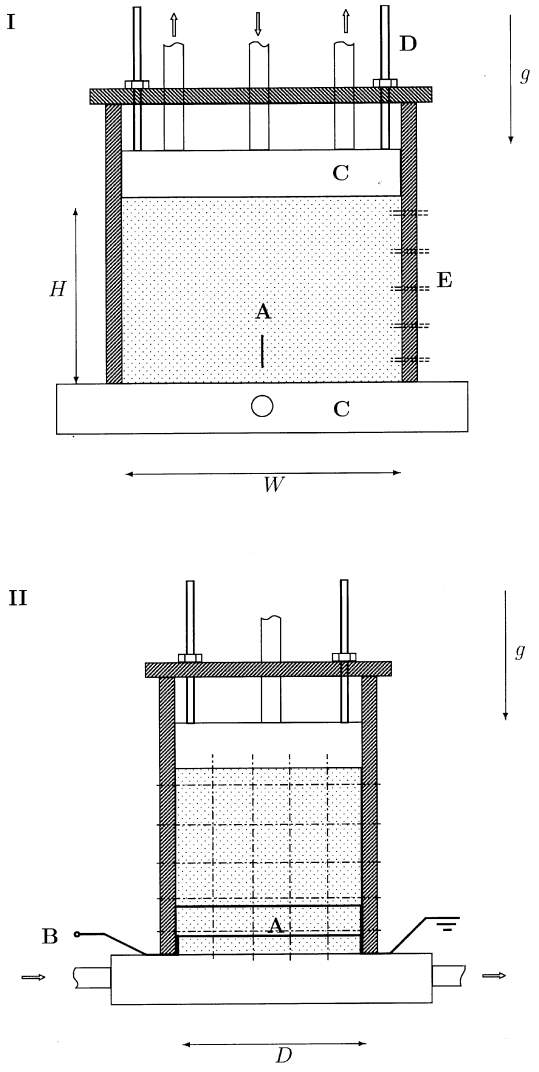

Fig. 1. The experimental setup: **I** front view, **II** side view; **A** heating element, **B** power supply, **C** heat exchangers, **D** aspect ratio adjustment, **E** probe access matrix.

in order to keep the temperature differences in the fluid within a range of 5 K.

The vertical orientation of the heat source yields a laminar plane plume release at a well defined, fixed position. The heating element consists of a customer specified flexible Kapton® heater[1] with a resistance of 5 Ω. Two strips of copper are stuck to the sides to decrease the flexibility. The orientation of the resistant material in the flexible heating strip is in longitudinal (D) direction. A direct current power supply is used with an adjustable range up to 50 V and 10 A.

The experimental cavity is equipped with confining top and bottom heat exchangers. The heat exchangers are supplied by water from a tank by a centrifugal pump at a rate of about $1 \cdot 10^{-4}$ m^3 s^{-1}. The height of the top heat exchanger is made adjustable and a small gap between the heat exchanger and the lateral walls is maintained. In this way the heating causes no hydrostatic pressure effects. From the heat exchangers the water flows back to the tank. The temperature in the tank is controlled by a Julabo P1 thermostatic heater in combination with a cooler. The volume of the tank is approximately 0.1 m^3 and the power of the heater is 1.6 kW. The cooler consists of a coiled copper tube, connected to the water grid, supplying water at a temperature of ca. 14°C and at a rate of $2 \cdot 10^{-4}$ m^3 s^{-1}. Thus, the temperature in the heat exchanger circuits is kept constant. Under the experimental conditions there is no problem in attaining a constant temperature with an accuracy of 0.1°C.

The side walls of the confinement are made of 0.1 m thick glass. With the use of glass the flow domain is optically accessible. This is required for the performance of shadowgraphy and PTV. The thickness of the walls ensured a heat loss through the sides, relatively small compared to the controlled heat exchange through top and bottom walls. In case of the maximum heating rate of 500 W, in the statistically steady state, the heat losses through the side walls are estimated to be 2%. This relative amount of heat loss may be assumed to be constant, also at lower heating rates.

As a successor of previously utilized setups the presently used configuration is empirically optimized as to possess a relatively high reproducibility of the observed flow phenomena. Top and bottom heat exchangers offer the feature of adjusting a prescribed homogeneous temperature at the start. Furthermore, after establishment of a re-circulating plume flow, top cooling provides a downflow centred around the rising plume. The present configuration creates a symmetrical mean flow. The bottom heat exchanger enforces a stratification up to the re-circulating convection region. The heat source is embedded in the stratified layer. Together with the vertical orientation of the source this results in a well defined vertical plume release.

4.2. Experimental conditions

In order to find the transitional flow regime, shadowgraphy is used to adjust the heat flux by visual inspection of the resulting qualitative projection. In this way the required heat flux can be adjusted. Having this heat flux, the transition is positioned at approximately half way the vertical extent of the flow domain.

Using the present configuration, the Rayleigh number as defined by

$$Ra = \frac{g\beta q' H^3}{\lambda \nu \kappa} \tag{13}$$

could be varied from zero to $4.6 \cdot 10^{11}$ at an ambient temperature of 20°C and to $1.0 \cdot 10^{12}$ at a temperature of 35°C. At the maximum heating rate the mentioned temperatures correspond to the start of the experiment and the equilibrium temperature, respectively. At the start of the actual experiment the temperature of the water in the setup was 19.5°C. The heat exchangers were kept at 19.5°C and the ambient temperature in the laboratory was 19.9°C. The power supply is turned on at a heating rate of ± 1102.5 W m^{-1}. Using the given heating rate, the dimensionless governing parameters are $Pr = 7.0$ and $Ra = 2.1 \cdot 10^{11}$, defined at a reference temperature of 20°C.

During the experiment the mean temperature in the setup rises. Due to this temperature increase Ra will increase and Pr will drop. At the start the heating element has to warm up before it begins to emit the heat to the water. The time constant of this starting effect can be estimated by $\tau_{el} = \rho c_p V/\alpha A$. Measurement of the temperature increase of the source yielded a value of 1.5 s, defining an average heat transfer coefficient α.

Starting the experiment the setup was filled with demineralized and de-aerated water. The temperature control in the heat exchangers supply tank was turned on, together with the flow through the heat exchangers. This situation was maintained for about two hours, spanning the time before the actual start of the experiment. This time span is needed to obtain a hydro-dynamically stagnant and thermally homogeneous initial condition.

A vertical cross-section of the resulting flow was recorded on video-tape using the PTV, and temperatures were measured with thermocouples at several locations. The experiment lasted for 600 s, assuring to have enough data in order to pass a transient of the flow field and to sample sufficient integral time scales to analyze the statistically stationary flow. Flow statistics as presented in this paper are obtained from the video recordings in the time interval [80–600] s.

[1] Kapton is a registered trademark of E. I. DuPont Company.

5. Particle tracking velocimetry

5.1. Introduction

The PTV is performed with the computer package DigImage as a basis ([5]). A detailed description of the optical arrangement and the applied tracking algorithm is given in [2].

At the moment the first results of 3-D velocity measurements appear in literature. The resolution of these measurements is relatively low. For the time being, in reducing experimental and data processing complexity, 2-D measurements are preferred. From 2-D data, spatial derivatives and 2-D dynamics can still be obtained, a main advantage of field measurements. Besides the present method, [5], for an overview of image analysis techniques the reader is referred to [1], [14], and [23].

In the PTV experiments the spatial sample resolution is not sufficient to represent the dissipation range. Resolving this range would imply a sample spacing that is equal to, or even smaller than the Kolmogorov scale. This is not a drawback in the perspective of the present study. The purpose of this study involves the validation of LESs and the testing of SGMs. The objective of LES is to represent only the energy containing eddies with sufficient accuracy.

5.2. Data processing

The raw data obtained from the tracking algorithm are processed with three objectives: (i) enlarging accuracy, (ii) spurious vector removal and (iii) interpolation on a square lattice. The present processing of the raw data will be outlined briefly. For a more extensive description the reader is referred to [2].

The localization procedure to determine the position of the particles has some finite accuracy limited by the image resolution and the size of the particles. At low velocities the localization accuracy determines the accuracy of the velocity. Therefore the velocity of a particle obtained between subsequent matchings is averaged. In the present study the averaging procedure covers five matchings, as motivated in the next section. Hence, particles that cannot be matched this number of times are eliminated.

The occurrence of unphysical or spurious vectors, as obtained from the particle tracking algorithm, is practically unavoidable. To get rid of these spurious vectors a filter is used based on a certain maximum allowable amount of variation within a searching area. The variation criterion is chosen to be twice the standard deviation. More specifically, the following steps are taken. For a particle i all other particles are determined that lie within a certain distance r_f from particle i. Then the averages ($\mu^i_{u_1}$ and $\mu^i_{u_3}$) and the standard deviations ($\sigma^i_{u_1}$ and $\sigma^i_{u_3}$) of the individual velocity components are determined over this set of particles, including particle i. Subsequently the length of the actual velocity deviation of particle i with respect to its neighbourhood is computed, according to

$$\sigma^i_{\text{test}} = \sqrt{(u^i_1 - \mu^i_{u_1})^2 + (u^i_3 - \mu^i_{u_3})^2}. \tag{14}$$

This is compared to the length of the standard deviation of the vector components for the region under consideration,

$$\sigma^i = \sqrt{(\sigma^i_{u_1})^2 + (\sigma^i_{u_3})^2}. \tag{15}$$

If the actual deviation σ^i_{test} is larger than twice the standard deviation σ^i the vector is removed from the data field. For a Gaussian distributed field this means that 5% of the data will be removed, even when there are no stray vectors. Experience turns out that the amount of stray vectors does not exceed 5% so that two times the standard deviation is a proper choice. The radius of the area taken into account, r_f, is determined by the amount of data found in each area. A very small amount of data may lead to non-significant statistics. On the other hand we want to preserve the local phenomena, so that the area may not be too large. A radius r_f of about 5% of the characteristic domain size is found to give good results.

For the interpolation of the unstructure field data to a grid, an algorithm as used by [22] is employed. The main interesting features of the interpolation are twofold. It does not show spurious oscillations as do high-order polynomial interpolations. Besides, the interpolation gives the exact measured value at the particle locations. Before carrying out the interpolation, boundary conditions are supplied by adding zero velocity vectors at equidistant positions along the walls.

5.3. Error estimation

The accuracy of the particle tracking algorithm is mainly determined by the accuracy of determining a particle position, the particle sedimentation velocity and the particle response to acceleration. The physical domain with an extent of 0.3 m is depicted on the image plane with an extent of 512 pixels, having about 1700 pixels m^{-1}. The typical accuracy of the localization of a particle with a size of about 3 pixels in each direction is 0.1 pixel ([5]). This yields a position accuracy of $\sigma_x = 0.1/1700 = 6 \cdot 10^{-5}$ m. Having accurately spaced samples in time with interval $\Delta t = 0.04$ s, thus, an accuracy for the velocity of $\sigma_u = 0.0015\ \text{m s}^{-1}$ is found. Using statistics, or a convolution of the velocity field over N_s samples in time, leads to a standard deviation of $\sigma^{N_s}_u = \sigma_u/\sqrt{N_s}$. If the highest occurring frequency suffices $f_{\max} \leqslant 1/(2N_s\Delta t)$ still a temporally resolved velocity is obtained. A value $N_s = 5$ for averaging the determined instationary velocity field yields an accurate description of the flow, as outlined in [2]. In the present measurements about 1000 particles were found in each frame, of

which 500 could be tracked over $N_s = 5$ frames. Thus, the mean spatial resolution is determined by these 500 particles with a mean mutual distance of about 10^{-2} m. The velocities are interpolated to a finer grid, containing 63×42 equidistant grid-points.

The sedimentation of the particles due to a slight density difference between particles and working fluid can be estimated by balancing the particles gravitational force with the Stokes drag. Since the particles are nearly spherical and the particle Reynolds numbers are lower than unity, this is a good guess. The estimated accuracy of the velocities σ_u due to the sedimentation speed u_{ps} then becomes:

$$u_{ps} = \frac{\rho_p - \rho}{\rho} \frac{g d_p^2}{18\nu}. \tag{16}$$

This yields a value of $\mathcal{O}(10^{-4})$ m s^{-1} which is an order below the value due to the localization accuracy. The response of a particle to a sudden acceleration can be determined by balancing the Lagrangian instationary forces on the particle with the Stokes drag. This gives a first-order integrating response with a typical reaction time given by:

$$\tau_a = \frac{\rho_p d_p^2}{18\rho\nu} \tag{17}$$

which is as large as $\mathcal{O}(10^{-3})$ s, being considerably smaller than the temporal sample spacing.

6. Data analysis

The obtained vector fields were interpolated on a staggered grid of size 63×42, yielding a spatial grid width of $\Delta \approx 4.76 \cdot 10^{-3}$ m. These steps are performed according to the method discussed in the previous section. By employing the temporal averaging over five samples the final resolution in time was 5 Hz, sampled at 25 Hz. The number of fields on which the analysis thus is constituted amounts to 2600 velocity fields. The 2-D plane in which the velocities are measured contains a horizontal and a vertical component that are indicated by u_1 and u_3, respectively.

Before analyzing the data any further the field was pre-filtered, resulting in a non-staggered velocity field, conserving the spatial sample spacing. This was performed with a trapezoidal rule over two points, that confine a volume. The reason for the application of a pre-filtering procedure is to obtain consistent filtered fields at different filter levels, of size Δ, 2Δ and 4Δ. The Δ level defines the small scales, the 2Δ level is connected to the grid scale in an LES and the 4Δ level is the test scale as defined in the dynamic procedure. From the Δ scale coarser scales are obtained by subsequent filtering using an extended trapezoidal rule (over nine points), the discrete approximation of a top-hat filter, conserving the sample spacing. This strategy is consistent with an actual LES employing a finite volume method on an equidistant grid.

By integrating the 2-D velocity divergence over discrete volumes of size 2Δ, an estimate can be obtained of the velocity differences $\Delta u_2(2\Delta)$ in source axial direction. The axial velocity difference is given by

$$\begin{aligned}\Delta u_2(2\Delta) = &(u_1(x_1+\Delta, x_2, x_3) - u_1(x_1-\Delta, x_2, x_3)) \\ &+ (u_3(x_1, x_2, x_3+\Delta) - u_1(x_1, x_2, x_3-\Delta)).\end{aligned} \tag{18}$$

From the 2-D measurements only three of the six subgrid stress components can be determined: τ_{11}, τ_{13} and τ_{33}. The trace of the subgrid scale stresses constitutes a grid scale pressure, which is incorporated in the already existing pressure term, in an actual LES. Therefore, in the comparison with subgrid stress models later on, one should look at the deviatoric part of it. This is not possible since the measurement is only 2-D. While this affects the τ_{11} and τ_{33} components, the value of τ_{13} will stay uncontaminated. Since the normal subgrid stress in axial direction τ_{22} cannot be determined in a straightforward way, the analysis will be kept 2-D. This yields for the 'exact' deviatoric subgrid stresses

$$\tau_{ij}^d = \tau_{ij} - \tfrac{1}{2}\tau_{kk}\delta_{ij}. \tag{19}$$

This strategy would be identically equal to an application of the assumption $\tau_{22} = (\tau_{11} + \tau_{33})/2$. The two known normal stresses τ_{11} and τ_{33} thus become exactly the opposite of each other. This procedure, therefore, would result in a loss of information and this is why the stresses will be presented with full trace. To be consistent also the window stresses, $\mathscr{L}_{ij}$, in the dynamic model are evaluated in this way.

To calculate the model stresses according to both the Smagorinsky and the dynamic model the magnitude of the rate of strain tensor, $|\bar{S}|$, has to be known. From the zero divergence of the incompressible flow field the normal unknown component can be calculated according to $\bar{S}_{22} = -(\bar{S}_{11} + \bar{S}_{33})$. The unknown components $\bar{S}_{12}$ and $\bar{S}_{23}$ are estimated to be equal to $\bar{S}_{13}$, following [18]. Furthermore, the subsequent filtering with a top-hat kernel results in a field at the test scale that is effectively filtered with a trapezoidal kernel with an effective width somewhat larger than $\hat{\Delta}/\Delta = 2$. In evaluating M_{ij} this is accounted for using the optimal effective value for the grid-ratio of $\sqrt{5}$ as derived by [31].

Also not all components involved in the contraction (12) are known. Here only contributions from the known components are taken into account. It is hardly possible to make some proper assumptions to estimate the unknown components of τ_{ij} and $\bar{S}_{ij}$. To make a just interpretation of the energy transfer possible such a blurring would be unwanted. Again, as in [18] the trace of the stress tensor is not subtracted here.

7. Results

7.1. *Mean flow*

A vector plot of the time mean flow is given in Fig. 2. A nearly symmetrical flow pattern is established, consisting of a plume that drives a circulation pattern in the upper half of the setup. By using a turbulent entrainment assumption, as outlined in [29], the magnitude of the mean flow can be estimated. The entrainment is defined as the time mean velocity or amount of fluid, entering the plume laterally by turbulent motion. For the present case (see [2]) an estimation of the mean upward flow in this way gives not very accurate results because in the laminar part there is no turbulent entrainment and the turbulent part is very much influenced by the presence of the confining top wall. The width of the plume suddenly increases as the bulk of re-circulating fluid entrains it at half the setup height. Here, the mean flow towards the plume is directed almost perpendicular to it. Below this level the entrainment is much smaller and the fluid does not flow horizontally towards the plume anymore. In this region the fluid is bent downwards before the attraction to the plume becomes large enough.

In fact the time mean flow clearly characterizes the spatial transition of the flow. At the height where the entrainment increases at an appreciable rate, the flow may be defined as spatially transitional. It turns from laminar, below this location, to turbulent, above it. Though the fluctuations of the vertical velocity are large already directly above the source, this does not indicate turbulence at this elevation yet. A small oscillation of the laminar plume causes this behaviour. The oscillations are irregular although the plume is still laminar. A sample sequence of the temperature at a point located at [0.15, 0.12, 0.10] m (from the left–front–bottom corner) is given in Fig. 4.

The irregular oscillations are nearly always present. They are mainly due to upstream influences and turbulence which is convected back to the source region. Arriving there, this turbulence possesses a reduced but still noticeable kinetic energy, still being able to determine the lateral motions of the laminar plume. This influences the more severe disruptions of the flow upstream and therefore the transitional process.

It was found ([2]) that the mean velocity profile in the lower plume part is relatively low and wide compared to results obtained from both laminar boundary layer assumptions and turbulent entrainment assumptions. As argued in [2] the flow in this region can be described as an irregularly oscillating laminar plume flow, yielding this striking result.

7.2. *Flow fluctuations*

An impression of the instationary behaviour of the flow is best obtained by looking at a shadowgraph. Employing this technique, it is observed that a transitional flow as obtained with the present configuration is highly intermittent. Two coherent phenomena can be discerned quite clearly. In a relatively large part of the time an oscillation is present in the thermal plume. The spatial start of this oscillation moves irregularly along the laminar plume. Also this structure ensemble sways and twists irregularly. At a few moments in time an alternating shedding of vortical dipolar structures can be observed. This was

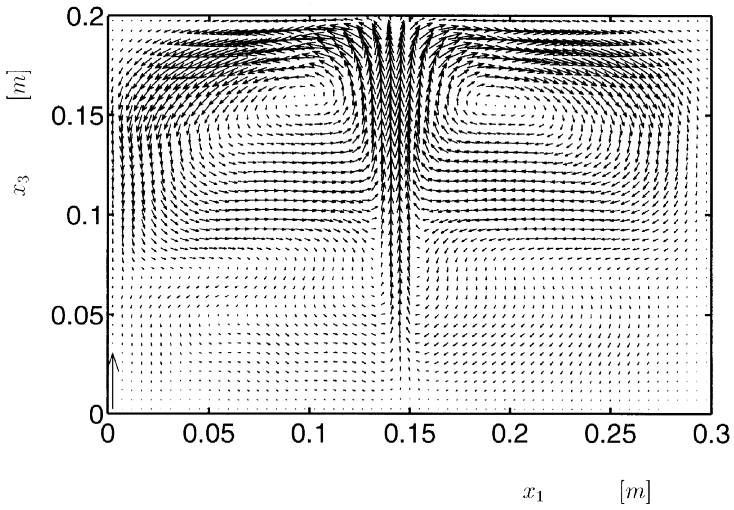

Fig. 2. Mean flow velocity vectors at $x_2 = \frac{1}{2}D$ as obtained by PTV. Flow parameters at starting conditions: $Ra = 2.1 \cdot 10^{11}$ and $Pr = 7.0$. Scaling: 0.01 m s^{-1} magnitude is displayed by the left-bottom vector.

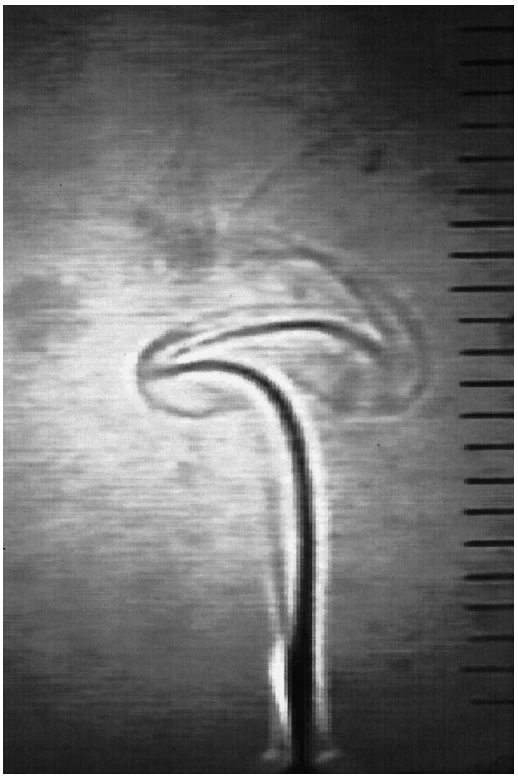

Fig. 3. Typical vortex shedding transition phenomenon.

most profound in experiments with an adiabatic top wall, as performed by [30]. In this case there is no buoyancy produced by a cooling top wall and a stable thermal stratification influences the flow field. This phenomenon was also observed by [24]. A typical example of the latter phenomenon is given in Fig. 3. Both phenomena occur irregularly in time and space.

The convergence of the flow to a steady state is checked by inspection of the low order statistics of the PTV velocity results as function of time. The velocities were taken at the midpoint because of our interest in the transitional region. These statistics should approach a converged value, which is zero in case of the mean horizontal velocity component. The velocities in the middle, the time mean and the standard deviation of it, as function of time, are displayed in Fig. 5, as well as their probability densities. It shows that at the end of the experiment the statistics are nearly constant.

It seems that there exists a tendency consisting of a long term decrease of the mean and standard deviation of the horizontal velocity. At the same time these statistics for the vertical component seem to increase slightly. The latter is mainly caused by the temperature dependent properties of the working fluid. The deviation of especially the horizontal mean component may be caused by an asymmetry of the setup, including an installation orientation which is not level. On the other hand, the difference of the mean horizontal velocity with its expected ideal value at the end of the experiment, relative to its standard deviation is within 10%. This justifies a

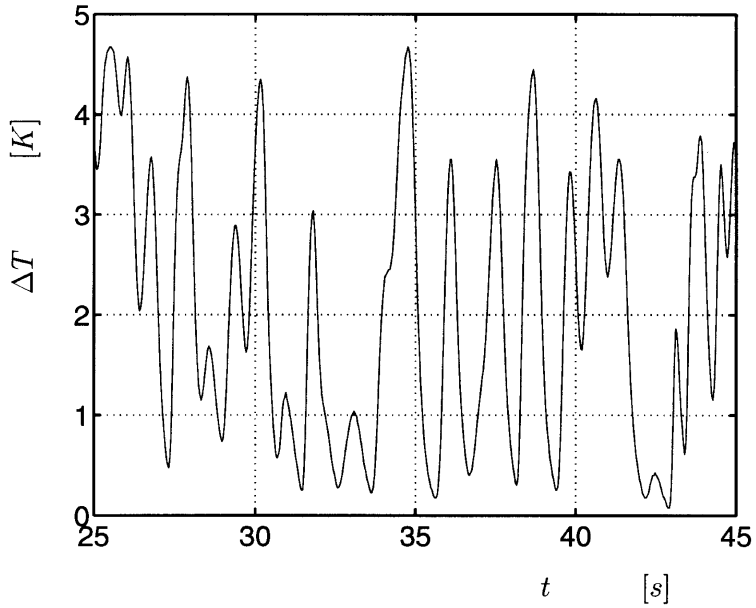

Fig. 4. Temperature record of the irregular oscillating plume at location [0.15, 0.12, 0.10] m.

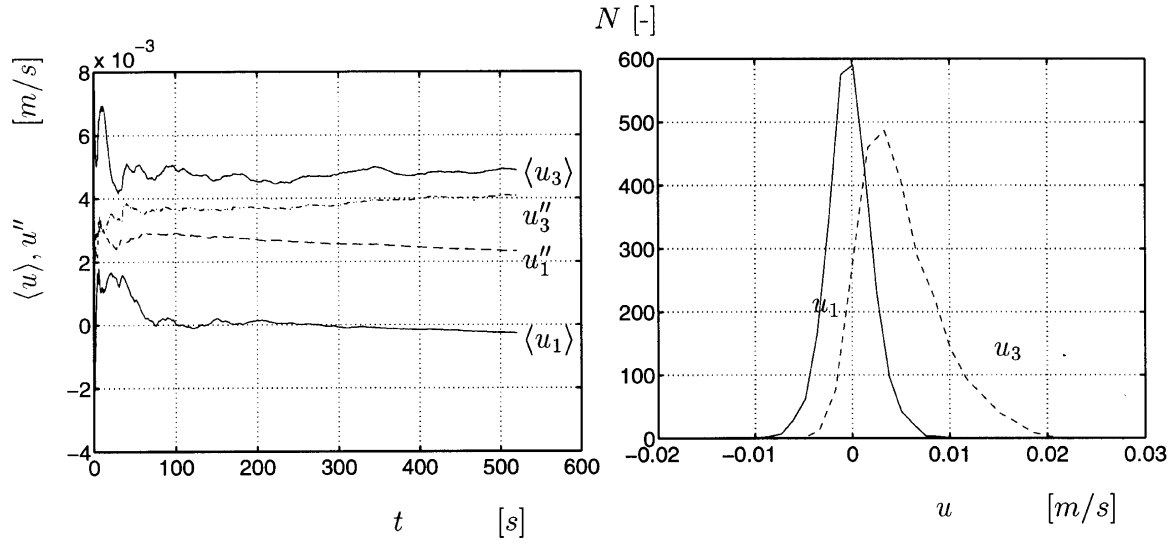

Fig. 5. Evolution of the statistics of the velocity components located at point [0.15, 0.10, 0.10] m as function of time (left), and their distributions (right).

qualitative analysis, not ascribing too much significance to the numerical value obtained.

The probability densities behave according to expectations based on physical grounds. Having no net forcing in horizontal direction results in a symmetrical distribution with mean zero, which is Gaussian-like. The distribution of the vertical component is positioned for the major part at positive values and it is skewed. The forcing, resulting locally in instantaneous strong updraughts, is responsible for both effects.

The spatial distribution of the fluctuations of the velocity components in the plane under consideration gives some insight into the turbulent behaviour of the plume. A contour plot of the standard deviations of the velocities is displayed in Fig. 6. These fluctuations in time are denoted by a double prime: u_i'', in contrast to time mean values that will be signified by angular brackets, e.g. $\langle u_i \rangle$. Due to lateral oscillations of the plume, the standard deviation of the vertical component u_3 is rather high already at small elevations from the heat source. Furthermore, its magnitude behaves like the mean vertical velocity. The fluctuations of the horizontal velocities u_1 are largest in the region where the lateral entrainment has a maximum.

The axial velocity difference $\Delta u_2(2\Delta)$ provides a measure of the three-dimensionality of the flow. The mean value and the standard deviation of this quantity are calculated and depicted in Fig. 7. The standard deviation of the axial velocity demonstrates evidently that the flow is 3-D. The frequency contents is similar to those in the other two directions.

From the velocity standard deviations the dissipation rate per unit mass can be estimated on the basis of an equilibrium range energy drain. Assuming a turbulent integral length scale l, it becomes: $\varepsilon \approx u_3''^3/l$. Employing an integral length scale $l = H$, the dissipation rate in the core of the plume reaches a value of $\varepsilon \approx 3.2 \cdot 10^{-7}$ m^2 s^{-3}. With this value, the micro-scales of length due to Kolmogorov and Taylor can be estimated to be: $(\nu^3/\varepsilon)^{1/4} \approx 1.3 \cdot 10^{-3}$ m and $u_3''\sqrt{15\nu/\varepsilon} \approx 2.7 \cdot 10^{-2}$ m, respectively. The spatial sample resolution of $\pm 10^{-2}$ m therefore is not enough to represent the dissipation range. This under the hypothesis that a 3-D equilibrium range would be present. However, the resolution is in accordance with the remarks as stated in the introduction and it resolves the energy containing eddies.

7.3. Subgrid stresses

The mean subgrid stresses and their standard deviations are depicted in Fig. 8, with full trace. The largest values of the subgrid stresses occur in the plume region, in which τ_{33} is particularly large. At the top wall high values of τ_{11} are present in the areas at which the plume spreads out to the left and to the right. Except for the top wall region these stress components correlate with the temporal standard deviations of the corresponding velocity components. The cross-component of the subgrid stress τ_{13} possesses much smaller values than the other two, the difference being an order of magnitude. This is caused by cancelling out of positive and negative contributions. High values of τ_{33} correspond with high values of the temporal standard deviation of the vertical velocity and are associated with small oscillating bound-

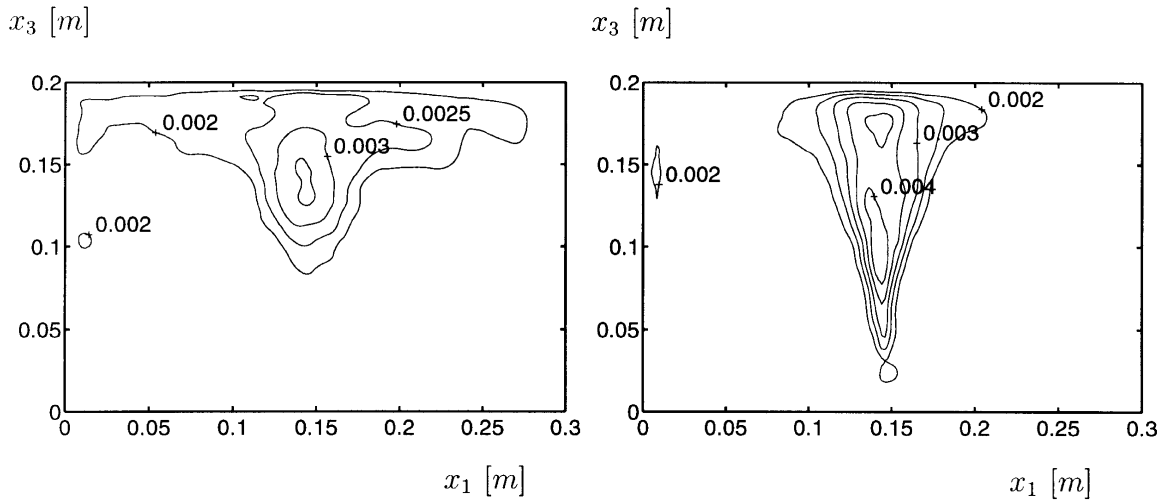

Fig. 6. Spatial distribution of the standard deviation of velocity components at $x_2 = \frac{1}{2}D$. Left: u_1'', right: u_3'', contour levels in m s^{-1}.

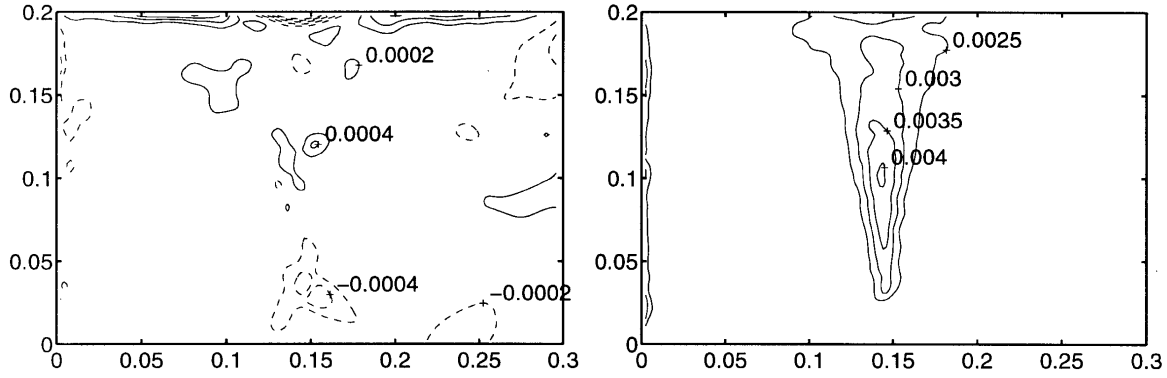

Fig. 7. Spatial distribution of the axial deviation of velocity components at $x_2 = \frac{1}{2}D$. Left: $\langle \Delta u_2(2\Delta) \rangle$, right: $\Delta u_2''(2\Delta)$, contour levels in m s^{-1}.

ary layers, i.e. in the plume region. In the same way the large value of τ_{11} in the transitional region can be explained by the occurrence of relatively small entraining regions.

Inspection of the standard deviations of the subgrid stresses shows that the fluctuations of all subgrid stresses are more equalized over the different components. They also have a more similar spatial distribution, except for the prominent fluctuations of τ_{11} at the top wall. It also shows that τ_{11} and τ_{33} remain positive most of the time, while τ_{13} more or less alternates around zero. On the other hand, the clear time mean τ_{13} behaviour suggests the existence of a coherent phenomenon. A real dissection into flow patterns would require a proper orthogonal decomposition, which is beyond the scope of the present study.

The large fluctuations at the left confining wall compared to those at the right wall may be caused by a set of physical and non-physical artefacts. The light sheet at the left wall was of a better quality compared to that at the right wall. Even with the use of local intensity equalization (after recording), this resulted in a larger number of particles detected at the left wall. In combination with instantaneously occurring large values of the second spatial derivatives near the wall this results in the large standard deviations of the subgrid stresses. Another reason might be the presence of reflection effects of particles at the confining glass surface. Occasionally a particle may be matched with its own reflection. However, the interest of the investigation is focussed on the plume region. In this area no spurious effects are observed.

The intensities and the mean of the Reynolds stresses are relatively small compared to the Leonard and cross stresses, as can be observed in Figs 9 and 10. Here devi-

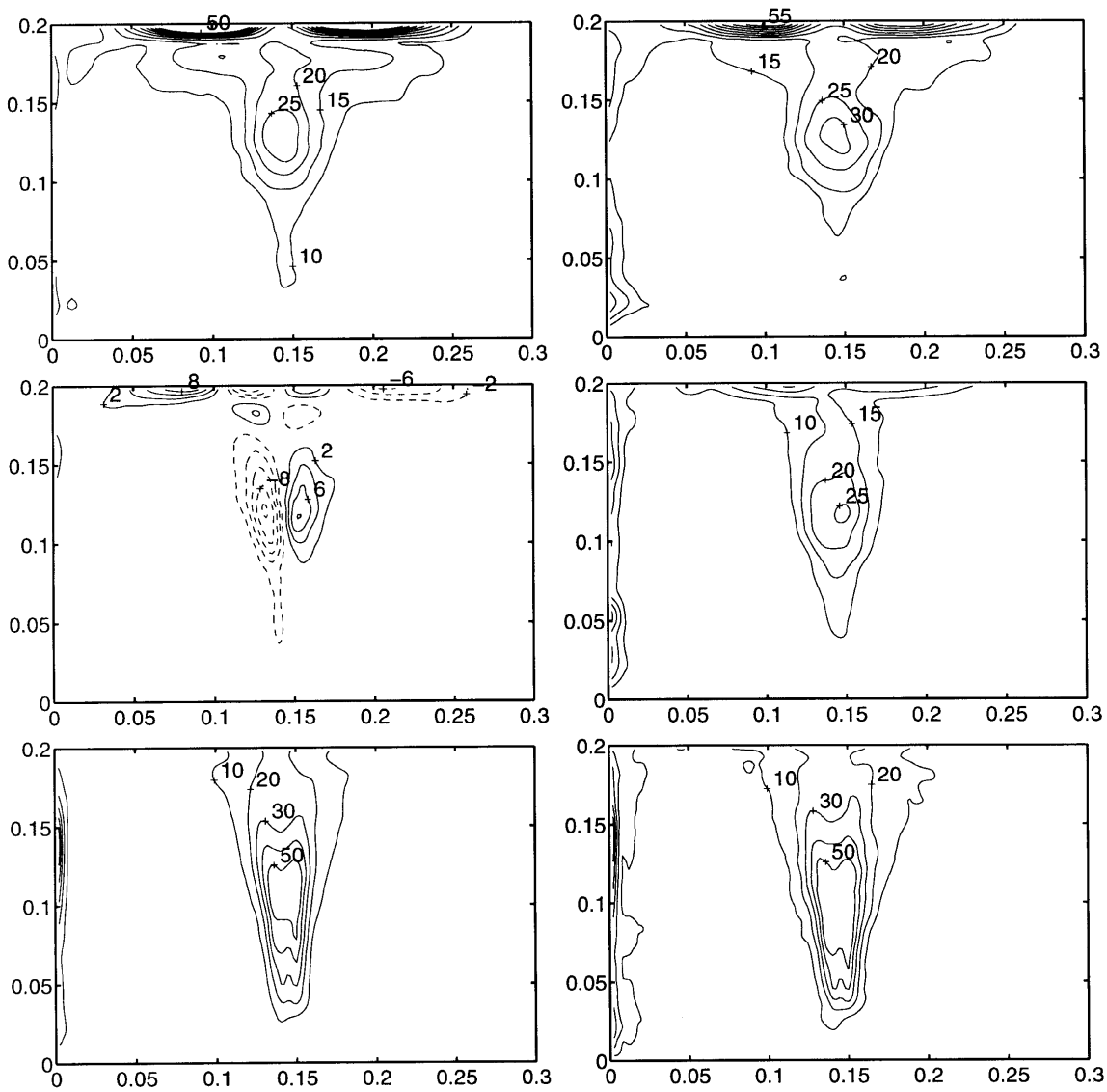

Fig. 8. Subgrid stresses at $x_2 = D/2$, top to bottom : τ_{11}, τ_{13} and τ_{33}, left : time mean stresses ; right : standard deviations. Levels multiplied by 10^7.

atoric parts are shown as outlined in the section considering the data analysis. The cross stresses are depicted in Fig. 11. Thus the fluctuations at the Δ level are much smaller than those at the 2Δ level. This is in accordance with a decreasing spectrum at larger wave numbers. However, for a 3-D equilibrium range, i.e. $E(k) \propto k^{-5/3}$, the expected difference in intensity amounts a factor $(\frac{1}{2})^{-5/3} = 3.2$. The observed difference, being a decade, would be in accordance with a spectrum with exponent $(^{10}\log(\frac{1}{2}))^{-1} = -3.3$ instead of $-5/3$. This suggests a 2-D turbulent inertial range around $k = \pi/2\Delta - \pi/\Delta$, according to [15]. Such an inertial range has an exponent equal to -3. Alternatively this behaviour could be due to the fact that this range of wave-numbers might lie in a dissipation range. On the basis of the estimation of the Kolmogorov microscale the latter hypothesis must be rejected. However, it is not yet very clear how the interpolation of the unstructured original data to a regular grid (with increased resolution on average) extends the spatial spectrum. It is this artefact that makes the above analysis a tentative exercise.

In the composition of the mean value of τ_{11} the influences of L_{11} and C_{11} are of equal and major importance. Since these components exhibit an almost equal standard

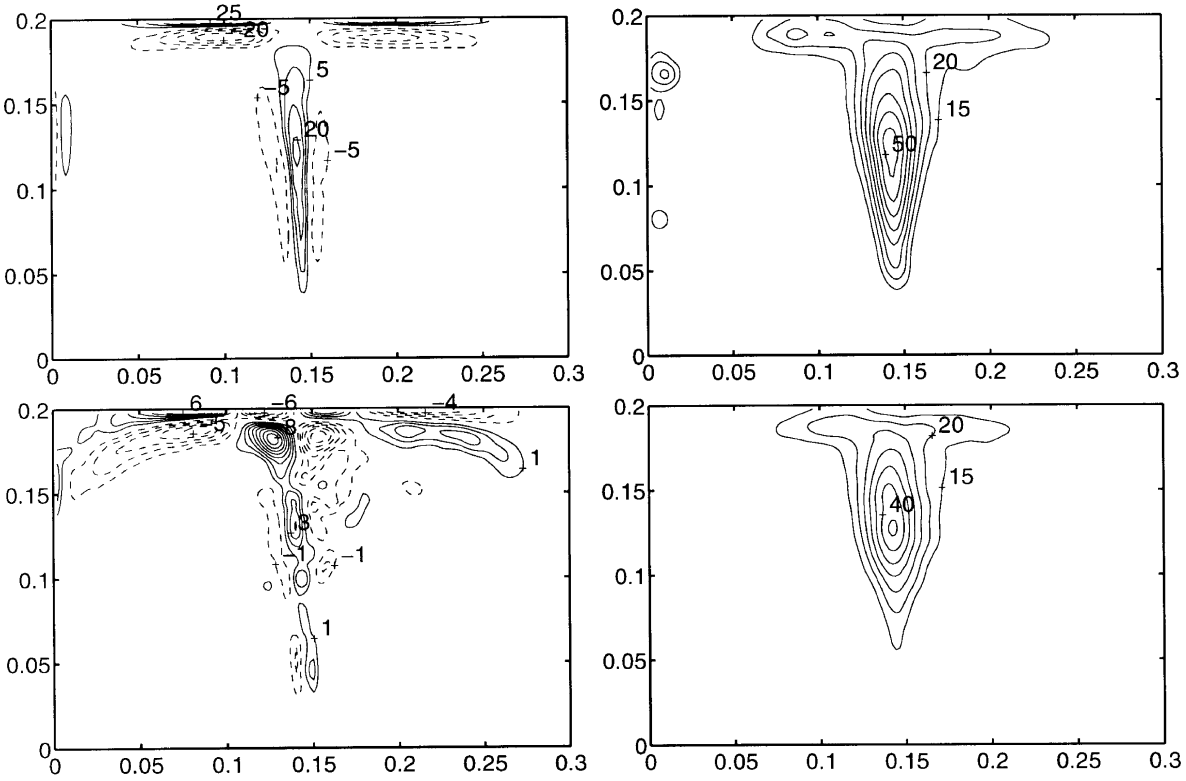

Fig. 9. Leonard stresses, deviatoric parts, top to bottom : L_{11}, L_{13}, left : time mean stresses ; right : standard deviations. Levels multiplied by 10^7.

deviation that is about twice as large as the standard deviation of the total stress, L_{11} and C_{11} must have a large negative correlation. For τ_{13} the influence of the Leonard term is particularly large in the top region, whereas the cross term is more profound in the lower plume region. According to the standard deviations here again a large negative correlation between Leonard stress and cross stress must be present. These negative correlations are also an attribute of 2-D motion as can be observed in a 2-D vortical flow field, e.g. given by $u_1 = \sin(2\pi k x_3)$, $u_3 = \sin(2\pi k x_1)$, which is also divergence free.

7.4. Kinetic energy transfer

In Fig. 12 the time mean kinetic energy transfer and its standard deviation are given. In the present case the length scale separating resolved components from subgrid components is defined with the filter width of 2Δ. The energy transfer thus defined is from scales above 2Δ to scales below this value. The mean kinetic energy transfer shows some regions with positive and negative values. If the turbulence was purely dissipative, only positive values would occur. In the plume region and near the top wall there are areas of negative energy transfer. This means that kinetic energy is transferred from small scales to larger spatial scales. This phenomenon is called 'backscatter'. It is expected that the occurrence of backscatter disqualifies subgrid scale models that are based on a statistical equilibrium assumption.

The time mean backscatter here originates from the injection of kinetic energy at a scale that is smaller than 2Δ. It has to be kept in mind that because of this a dissipative drain of kinetic energy might be present also below this 2Δ level. Most of the kinetic energy is present in the lower wave-numbers and must therefore be transferred from the high wave-numbers downwards.

Besides the time mean backscatter in the lower part of the plume, instantaneous backscatter occurs in the total up-flowing area. This is demonstrated by the standard deviation of the inter-scale kinetic energy transfer $\varepsilon''(2\Delta)$, together with the observation that the distribution of $\varepsilon(2\Delta)$ is not far from symmetrical. It shows that the instantaneous values are about ten times as large as the mean value. Thus backscatter and forward scatter are equally important phenomena in the plume region. Integrating the energy transfer and its standard deviation over the domain yields values of $1.0 \cdot 10^{-7}$ W m^{-1} and $3.5 \cdot 10^{-5}$ W m^{-1}, respectively. The latter was evaluated

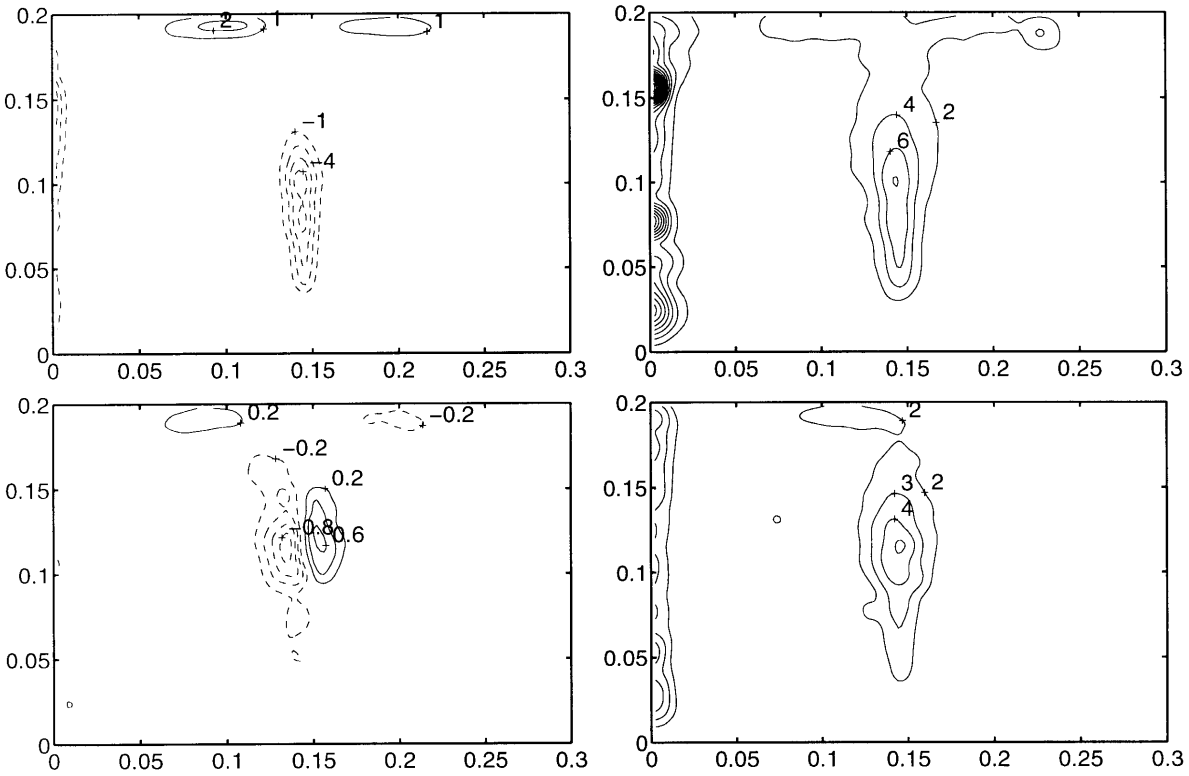

Fig. 10. Subgrid Reynolds stresses, deviatoric parts, top to bottom : R_{11}, R_{13}, left : time mean stresses ; right : standard deviations. Levels multiplied by 10^7.

over the region at the right from position $x = 0.043$. Therefore inter-scale kinetic energy transfer is much more important than the net kinetic energy drain. This is in qualitative agreement with results as found by analyzing forced convective flows resulting from direct numerical simulation, e.g. by [8] and [26], in the sense that backscatter is a possible physical feature.

It can be concluded that backscatter is essential in the present problem at the 2Δ level, especially when most of the fluctuations are to be simulated. At the Δ level the influence might be strongly reduced, although actual LESs on a Δ grid do not result in a satisfactory representation of the flow as indicated by [2]. A subgrid scale model should therefore exhibit the ability for providing backscatter. At least a reduction in subgrid dissipation to zero in laminar, i.e. resolved regions, is an advantageous property. Therefore dynamic modelling is preferred beforehand. However, at $Pr > 1$, as in the case of water, the modelling of the subgrid fluxes may be more critical.

7.5. A priori testing

On the basis of the filtered velocity fields the subgrid stresses are calculated according to the Smagorinsky model and the dynamic model. The objective of this analysis is to discern between the predictive qualities of the mentioned SGS models in a statistical sense. Thus, a realization at some point in time may yield a low correlation between predicted and exact subgrid effects. In the present study this constitutes a tolerable degree of freedom because most engineering flows are characterized with numerical methods far beyond any predictability horizon. However, low correlations of instantaneous stresses with model stresses indicate a poor performance of the model and are not very likely to produce satisfactory statistics.

The subgrid stresses as calculated on the basis of the Smagorinsky model are given in Fig. 13. The value of τ_{13} as determined by this model is similar to the 'exact' subgrid stress, except for the top wall region in which the predicted stress is opposite to the real stress. Qualitatively the fluctuation of τ_{13} and τ_{33} as predicted by the Smagorinsky model agrees fairly well with that obtained by grid-scale information. In the plume region the time mean τ_{11} and τ_{33} components are in disagreement with the exact values. Results for the dynamic model are depicted in Fig. 14. Application of this model to filtered data yields better results for the τ_{11} and τ_{33} components, though the

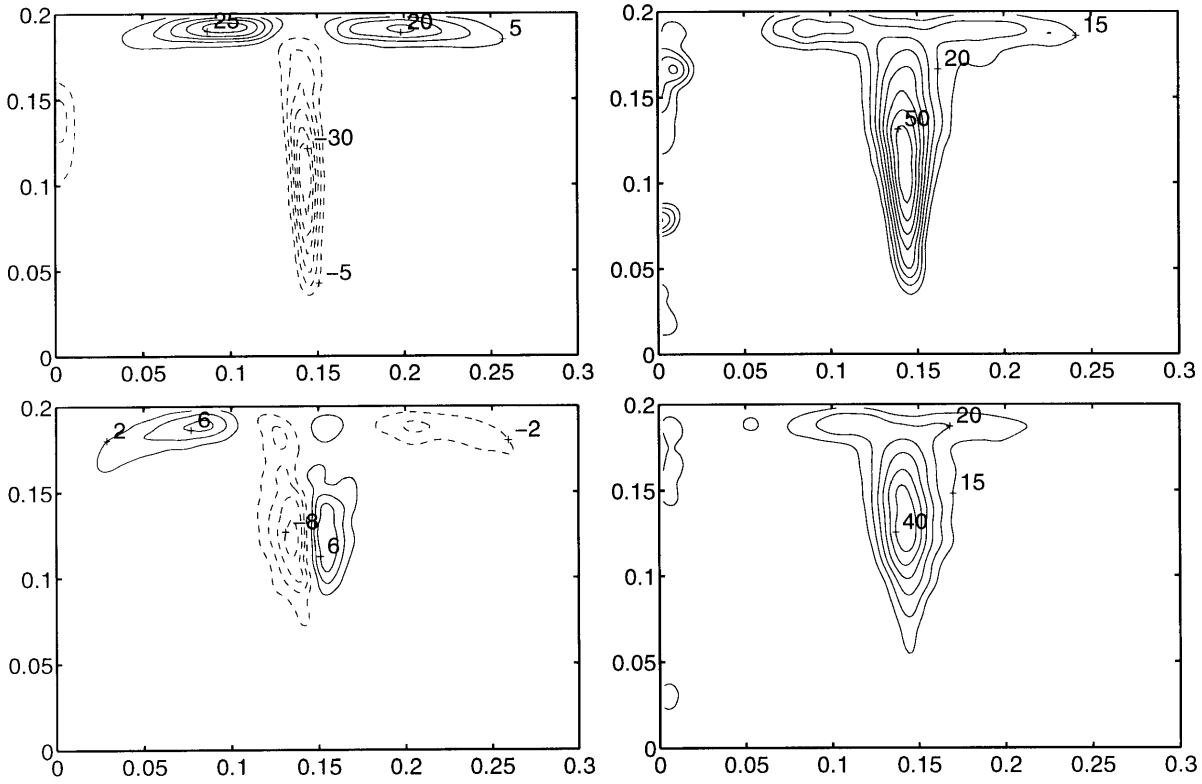

Fig. 11. Subgrid cross stresses, deviatoric parts, top to bottom: C_{11}, C_{13}, left: time mean stresses; right: standard deviations. Levels multiplied by 10^7.

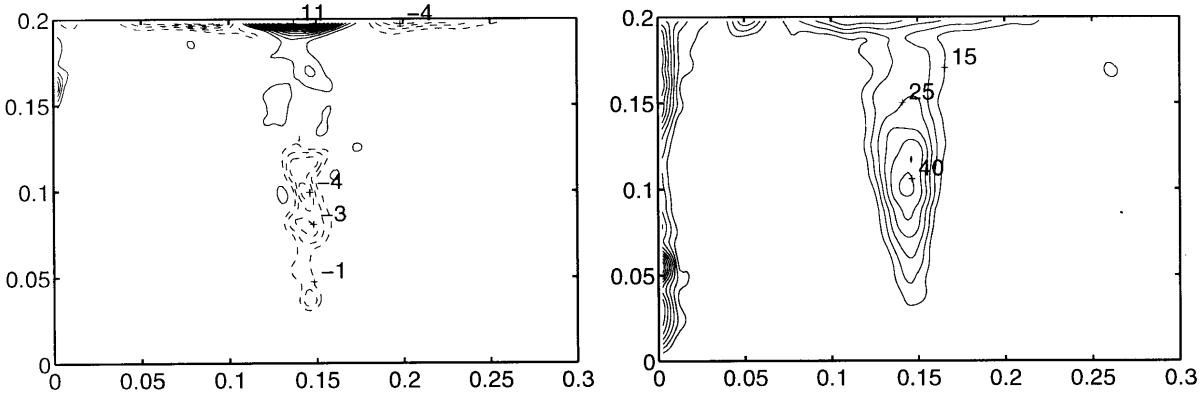

Fig. 12. Kinetic energy transfer $\varepsilon(2\Delta)$ at $x_2 = \frac{1}{2}D$, left: time mean, right: standard deviation. Levels multiplied by 10^7.

agreement is still very poor. For τ_{13} the dynamic model predicts opposite values and the temporal fluctuations of all components are underestimated.

Contrary to the subgrid stresses, the inter-scale kinetic energy transfer as obtained by the dynamic model gives results that are very similar to the exact transfer rates. This energy transfer is depicted in Fig. 15, and has to be compared to Fig. 12. A good quantitative agreement for the mean inter-scale kinetic energy transfer is obtained if the dynamic procedure is applied, though the result near no-slip walls depends heavily on the implementation of the dynamic procedure. Boundary conditions for the filtering operations have to be applied. The standard deviation of the kinetic energy transfer is estimated to be half

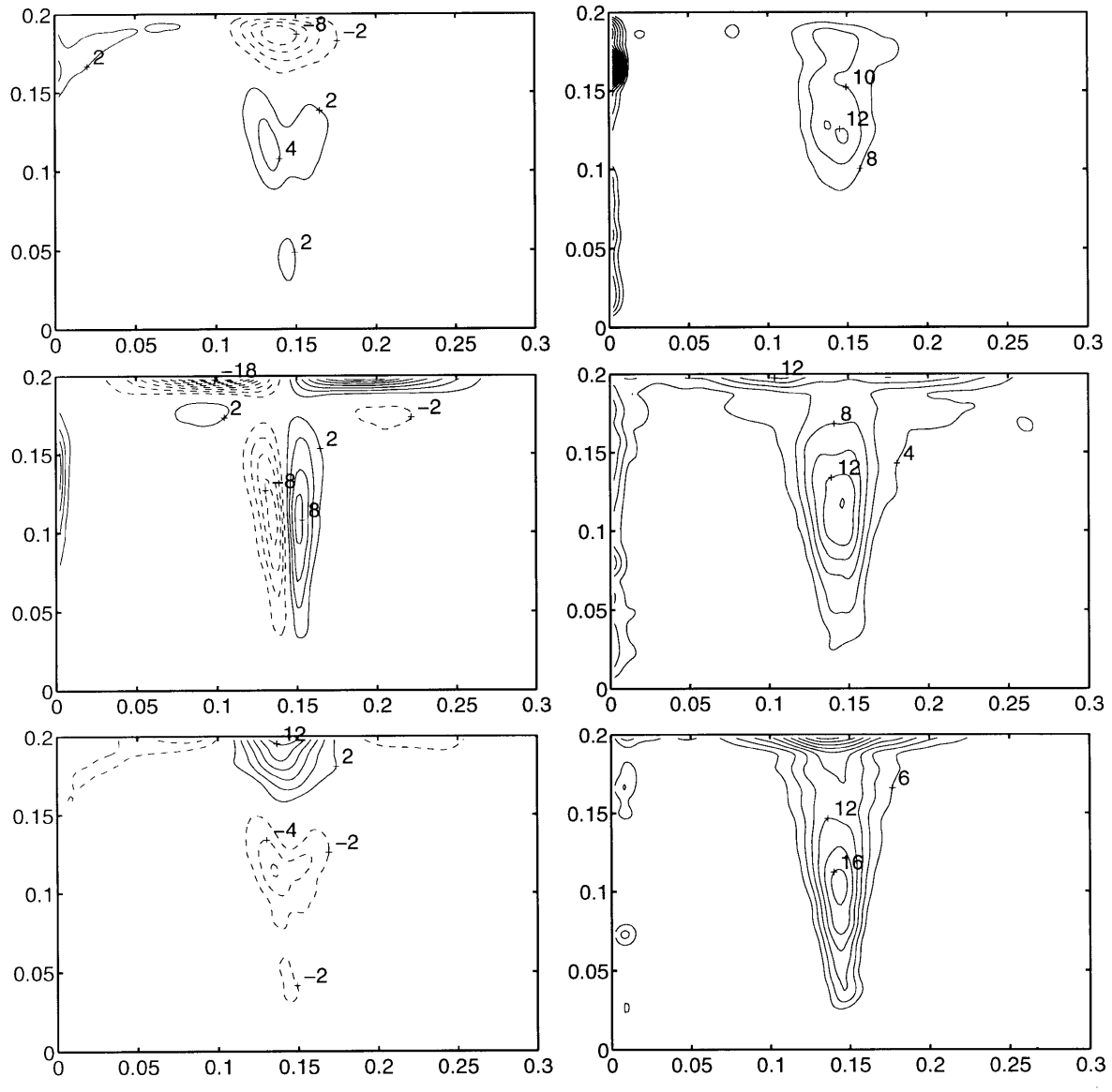

Fig. 13. Subgrid stresses, based on the Smagorinsky model, top to bottom: τ_{11}, τ_{13} and τ_{33}, left: time mean stresses; right: standard deviations. Levels multiplied by 10^7.

of the exact standard deviation. It seems that the effective resolution of subgrid stresses and grid-scale strains differs somewhat, causing the distinction.

In evaluating $\mathscr{L}_{ij}$ and M_{ij} the 2Δ hat filter has to be applied to several flow quantities. Therefore boundary conditions at the no-slip walls have to be met. Here it is assumed that all stresses and strains do not alter over the boundary. This is a logical consequence of the impermeable no-slip condition for the velocity components.

The dynamic parameter C is calculated at each point of the Δ grid. Afterwards it is filtered to the 2Δ grid. This is allowed since the parameter is defined on the basis of similarity between the 4Δ scale and the 2Δ scale. Therefore on the one hand a Δ resolution for C would not be representative. On the other hand, nearly singular values of C caused by an almost zero value of $M_{ij}M_{ij}$ are thus filtered out. Since the kernel of the filter exceeds the domain boundaries, a crucial aspect of the filtering operation here is the implementation of boundary conditions for C at the no-slip walls. Application of a homogeneous Neumann condition leads to the present results. One could also plead for a homogeneous Dirichlet condition

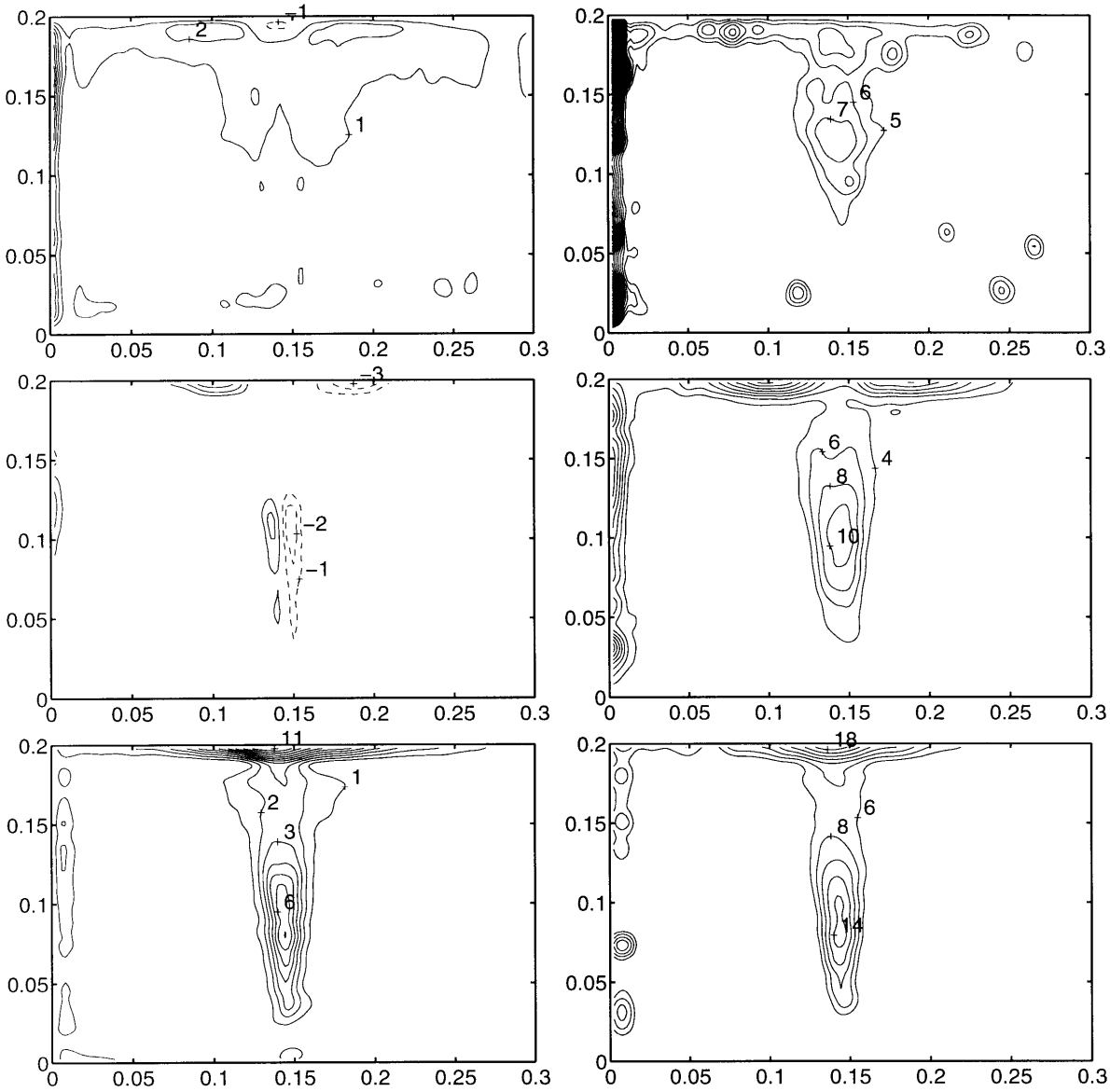

Fig. 14. Subgrid stresses, based on the dynamic model, top to bottom: τ_{11}, τ_{13} and τ_{33}, left: time mean stresses; right: standard deviations. Levels multiplied by 10^7.

since the flow is laminar at the wall. However, in an actual LES this is already obtained by setting the boundary condition for the eddy viscosity accordingly. A Dirichlet condition for C at the upper confinement causes the energy transfer to be limited too much.

The energy transfer determined with the Smagorinsky model results in values four orders of magnitude lower than the dynamic model for both the time mean and fluctuating transfer rates. The Smagorinsky model shows increased values at the top wall, being positive in this entire region. Relating the evaluation of the energy transfer, the Smagorinsky model is inferior comparing it to the dynamic model. Yet, in applying the dynamic model care must be taken in the application of appropriate boundary conditions at no-slip walls.

Evaluating the dynamic model on the experimental data reveals a value for the dynamic constant C, and thus for the Smagorinsky constant C_s as function of space. The statistics of the dynamic constant are given in Fig. 16. Here again the presence of backscatter is irrefutable.

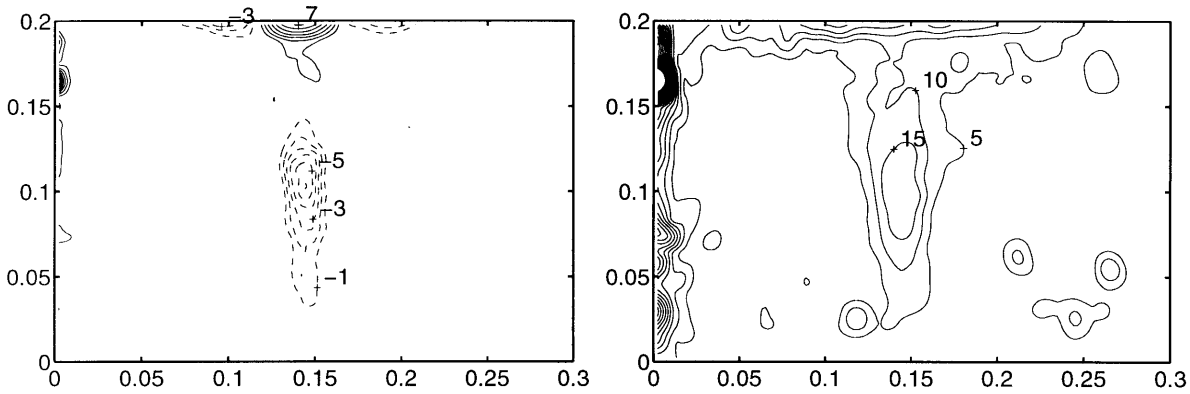

Fig. 15. Kinetic energy transfer $\varepsilon(2\Delta)$ at $x_2 = \frac{1}{2}D$ determined with the dynamic model, left: time mean, right: standard deviation. Levels multiplied by 10^7.

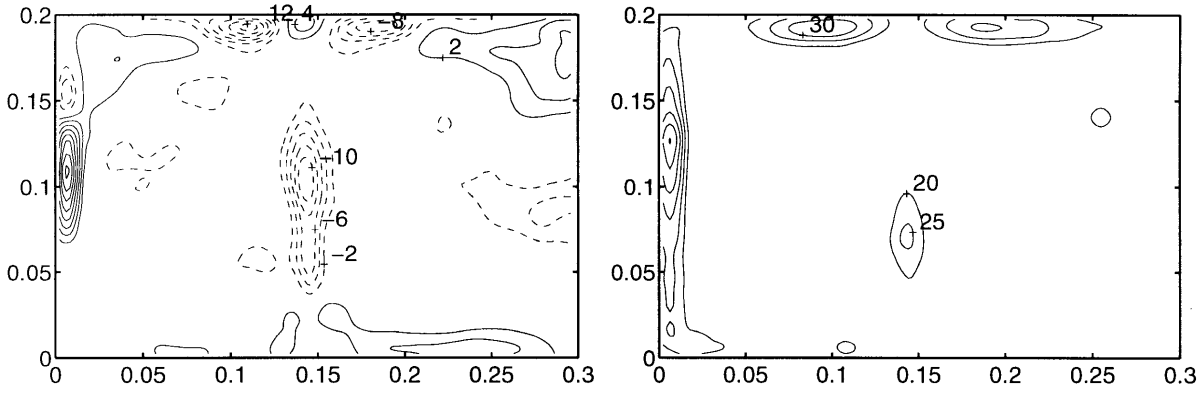

Fig. 16. Value of the dynamic parameter C at $x_2 = \frac{1}{2}D$, left: time mean, right: standard deviation. Multiplication factor 10^3.

In the plume region the dynamic constant has a minimal magnitude of -0.01, corresponding with a negative Smagorinsky constant of magnitude 0.1. The maximal fluctuation of the dynamic constant corresponds to a fluctuating Smagorinsky constant with amplitude 0.16.

8. Conclusions

A transitional plume flow was measured by means of particle tracking velocimetry. A converged representation of the flow statistics was obtained. The transitional region, defined by a sudden broadening of the mean flow, was located in the centre of the flow domain. Above the transition two re-circulation regions filled the upper half of the domain.

By applying a spatial filtering operation to the measured data, the exact subgrid contributions were determined as defined in the framework of LES. Subgrid models applied to the filtered field yielded data that could be compared to the exact contributions, in an a priori sense. A low correlation of time mean model subgrid stresses with exact subgrid stresses was found. In the transitional region the inter-scale kinetic energy transfer was found to possess a large standard deviation compared to relative low time mean values. Thus, in this region backscatter and forward scatter of kinetic energy are of equal importance. A qualitative good representation of the exact inter-scale kinetic energy transfer was obtained with the dynamic model applied to filtered data.

This study reveals that numerical prediction of the behaviour of transitional plumes originating from small buoyancy sources by means of LES is a very delicate affair. Globally this is due to three major causes. First, especially at high Prandtl numbers, care must be taken to resolve the thermal boundary layer as well as the hydro-dynamical boundary layer. Second, enough subgrid scales must be present to allow a statistical description of the flow. The last and most severe property a model should possess is the representation of the effects

of persistent backscatter. In many numerical methods backscatter, at a physically sufficient rate, is prohibited by numerical stability. In a posteriori tests the sensitivity of the results on the errors or uncertainties in the subgrid models can be tested. It is reported in [2] that actual LES with the models considered in this paper show a mean plume flow of which the mean speed is two to three times the measured value.

For the present configuration more research is required to investigate the behaviour of the subgrid buoyant fluxes. Here the hypothesis of the turbulent Prandtl number should be tested, and correlations of the fluxes with resolved quantities may indicate new modelling procedures. For the time being practical applications can be assessed by means of DNS of characteristic pieces of the flow problem, only evaluating the flow field in interesting parts of the domain, applying appropriate boundary conditions.

Acknowledgements

The authors are grateful to Mr G. A. J. van der Plas for the assistance in carrying out the experiment and the data processing and to Prof. F. T. M. Nieuwstadt for his contributions in the preparation of the manuscript.

References

[1] Adrian RJ. Particle-imaging techniques for experimental fluid mechanics. Ann Rev Fluid Mech 1991;23:261–304.
[2] Bastiaans RJM. Large-eddy simulation of confined transitional plumes. Ph.D. thesis, Eindhoven University of Technology, 1996. ISBN 90-386-0259-6.
[3] Bill Jr. RG, Gebhart B. The transition of plane plumes. Int J Mass Heat Transfer 1975;18:513–26.
[4] Clark RA, Ferziger JH, Reynolds WC. Evaluation of subgrid-scale models using an accurately simulated turbulent flow. J Fluid Mech 1979;91(1):1–16.
[5] Dalziel SB. Decay of rotating turbulence: some particle tracking experiments. In: Nieuwstadt FTM, editor. Flow Visualisation and Image Analysis. Kluwer Academic, 1993.
[6] Deardorff JW. A numerical study of three-dimensional turbulent channel flow at large Reynolds numbers. J Fluid Mech 1970;41:453–80.
[7] Desrayaud G, Lauriat G. Unsteady confined buoyant plumes. J Fluid Mech 1993;252:617–46.
[8] Domaradzki JA, Liu W, Brachet ME. An analysis of subgrid-scale interactions in numerically simulated isotropic turbulence. Phys Fluids A 1993;5:1747.
[9] Ducros F, Comte P, Lesieur M. Large-eddy simulation of transition to turbulence in a boundary layer developing spatially over a plate. J Fluid Mech 1996;326:1–36.
[10] Eidson TM. Numerical simulation of the turbulent Rayleigh–Bénard problem using subgrid modelling. J Fluid Mech 1985;158:245–68.
[11] Gebhart B, Jaluria Y, Mahajan RL, Sammakia B. Buoyancy Induced Flows and Transport. Hemisphere, 1988.
[12] Gebhart B, Pera L, Schorr AW. Steady laminar natural convection plumes above a horizontal line heat source. Int J Heat Mass Transfer 1970;13:161–71.
[13] Germano M, Piomelli U, Moin P, Cabot WH. A dynamical subgrid-scale eddy viscosity model. Phys Fluids A 1991;3(7):1760–5.
[14] Grant I. Selected papers on particle image velocimetry. SPIE Milestone series; MS 99. Bellingham, 1994.
[15] Kraichnan RH. Inertial ranges in two-dimensional turbulence. Phys Fluids 1967;10:1417–23.
[16] Lilly DK. The representation of small-scale turbulence in numerical simulation experiments. In: Proc of the IBM Scientific Computer Symposium on Environmental Sciences 1967;195–210. IBM Form No. 320–1951.
[17] Lilly DK. A proposed modification of the Germano subgrid-scale closure method. Phys Fluids A 1992;4(3):633–5.
[18] Liu S, Meneveau C, Katz J. On the properties of similarity subgrid-scale models as deduced from measurements in a turbulent jet. J Fluid Mech 1994;275:83–119.
[19] McMillan OJ, Ferziger JH. Direct testing of subgrid-scale models. AIAA J 1979;17(12):1340–6.
[20] Minev PD, van de Vosse FN, Timmermans LJP, van Steenhoven AA. A second-order splitting algorithm for thermally-driven flow problems. Int J Num Meth Heat Fluid Flow 1995;6(2):51–60.
[21] Moin P, Kim J. Numerical investigation of turbulent channel flow. J Fluid Mech 1982;118:341–77.
[22] Nguyen Duc JM, Sommeria J. Experimental characterization of steady two-dimensional vortex couples. J Fluid Mech 1988;192:175–92.
[23] Nieuwstadt FTM, editor. Flow Visualisation and Image Analysis. Kluwer Academic, 1993.
[24] Noto K, Honda M, Matsumoto R. Coherent motion of turbulent thermal plume in stably stratified fluid. Fluid Dyn Res 1988;3:415–21.
[25] Pera L, Gebhart B. On the stability of laminar plumes: some numerical solutions and experiments. Int J Heat Mass Transfer 1971;14:975–84.
[26] Piomelli U, Cabot H, Moin P, Lee S. Subgrid-scale backscatter in turbulent and transitional flows. Phys Fluids A 1991;3(7):1766–71.
[27] Piomelli U, Moin P, Ferziger JH. Model consistency in large-eddy simulation of turbulent channel flows. Phys Fluids 1988;31(7):1884–91.
[28] Rouse H, Yih CS, Humphreys HW. Gravitational convection from a boundary source. Tellus 1952;4:201–10.
[29] Turner JS. Turbulent entrainment: the development of the entrainment assumption, and its application to geophysical flows. J Fluid Mech 1986;173:431–71.
[30] van der Burgt TCG. Experimental analysis of a transitional plume. Master's thesis, Eindhoven University of Technology, The Netherlands, 1994. WOC-WET 94.015.
[31] Vreman AW. Direct and large-eddy simulation of the compressible turbulent mixing layer. Ph.D. thesis, University of Twente, The Netherlands, 1995.
[32] Wong VC, Lilly DK. A comparison of two dynamic subgrid closure methods for turbulent thermal convection. Phys Fluids 1994;6(2):1016–23.